sustainability

MDPI

Article

Effects of Dry-Wet Cycles on the Mechanical Properties and Meso-Fabric of Metal Tailings

Pengfei An [1], Zhijun Zhang [2], Yakun Tian [2,*], Min Wang [2] and Zhifeng Lin [1]

[1] School of Traffic Engineering, Huanghe Jiaotong University, Jiaozuo 454950, China; anpengfei5@foxmail.com (P.A.); 15039118269@163.com (Z.L.)
[2] School of Resources, Environment and Safety Engineering, University of South China, Hengyang 421001, China; 2003000550@usc.edu.cn (Z.Z.); wangmin@usc.edu.cn (M.W.)
* Correspondence: 2017000012@usc.edu.cn

Abstract

To investigate the effects of repeated drying and wetting on the mechanical properties and meso-fabric of metal tailings, lead-zinc tailings from Hunan Province were studied. A self-developed apparatus was used to simulate the cyclic drying-wetting processes. Combined with triaxial shear tests and stereomicroscopic image analysis, the changes in macroscopic mechanical properties and meso-fabric, as well as their correlation mechanisms, were investigated. The results indicate that the wet-dry cycles did not alter the strain-softening characteristics of the tailings' stress-strain curves; however, they significantly intensified the degree of softening during the later stages of cycling (4–6 cycles). The static strength exhibited a trend characterized by "initial gradual degradation → temporary recovery → further deterioration" with an increasing number of cycles. After six cycles, the strength was significantly reduced compared to the initial state. The effective cohesion (c') fluctuated markedly, with an amplitude of 31.1%, while the variation in the effective internal friction angle (φ') was only 6.02%, indicating that dry-wet cycles have a more pronounced effect on the cohesion of tailings. At the microscopic level, the dry-wet cycling process promoted the upward migration of fine particles ranging from 0 to 60 μm, resulting in a decrease in the proportion of smaller particles in the lower layer. The porosity increased overall, with the lower layer rising from 44.06% to 54.26%. Pore evolution was dominated by the enlargement of pores larger than 150 μm. The macro-meso correlation analysis revealed that "fine particle migration → expansion of pores → loss of cementitious material" was the core driving factor for the deterioration of macroscopic mechanics, and the macroscopic mechanical response was the external manifestation of the adjustment of the microscopic structure. This research can provide certain theoretical support for the long-term safe operation and stability improvement of tailings dams.

Keywords: metal tailings; dry-wet cycles; mechanical properties; meso-fabric

Check for updates

Academic Editors: Guannan Liu, Sheila Devasahayam, John Samuel Thella, Mohammadali Sepehri and Sela Akdag

Received: 20 November 2025
Revised: 7 January 2026
Accepted: 8 January 2026
Published: 2 February 2026

Copyright: © 2026 by the authors. Licensee MDPI, Basel, Switzerland. This article is an open access article distributed under the terms and conditions of the Creative Commons Attribution (CC BY) license.

1. Introduction

As a critical supporting facility in metal mining operations, tailings ponds can, in the event of a dam failure, trigger severe environmental disasters. Such accidents not only pose risks of significant casualties and property loss but may also lead to long-term environmental pollution, causing potentially irreversible damage to surrounding ecosystems [1–3]. However, driven by the principles of the circular economy, the resource utilization of tailings is emerging as an important pathway to enhance resource efficiency

and promote sustainable development [4–6]. Therefore, ensuring the safe storage of tailings and the long-term stability of tailings dams remains a core challenge in mining safety and environmental protection. Under natural conditions, tailings dams and stockpiles are subjected to long-term exposure to climatic factors such as rainfall and evaporation. These conditions cause the tailings materials to undergo repeated wetting and drying processes. Such cyclic actions may induce a range of complex physical, chemical, and mechanical responses, which can eventually lead to structural instability and pose risks to dam safety [7,8].

A number of studies have shown that repeated drying-wetting cycles can reduce key mechanical parameters of geotechnical materials, including compressive strength, tensile strength, and elastic modulus [9–13]. For instance, experimental work on sandstone revealed a clear decline in tensile strength as the number of cycles increased [9]. Similar trends have been observed in mudstone, where both strength parameters and failure modes deteriorate under cyclic drying and wetting [12]. Research on marine clay stabilized with steel slag further indicates that initial curing conditions and subsequent disturbances influence strength development [14]. Another important factor is the soil's hygroscopic water content; when the initial moisture exceeds the maximum hygroscopic water content, the effect of water on mechanical behavior changes notably [15].

The decline in macroscopic mechanical properties of geomaterials under drying-wetting cycles can be linked to micro- and meso-structural alterations, such as changes in pore structure, particle arrangement, and interparticle connections [16–19]. For example, mudstone samples tend to disintegrate progressively under cyclic conditions, producing fragments of various sizes—suggesting that structural breakdown at the particle scale contributes to macroscopic weakening [20]. SEM studies on loess have also illustrated microstructural evolution induced by wetting-drying cycles [21]. The presence and subsequent evaporation of water considerably affect interparticle mechanical behavior. In wet stages, water films may reduce intergranular friction or cementation strength, whereas drying can temporarily increase cohesion due to capillary forces. However, this temporary strengthening is reversible, and repeated swelling and shrinkage tend to damage the original cemented fabric [22]. In red-bed soft rock, drying-wetting cycles lead to micropore development and detachment of fine particles, resulting in nonlinear growth in porosity and a shift toward larger pore sizes [23]. Similarly, water erosion in cemented broken mudstone raises both porosity and permeability, with pore connectivity improving as cycles proceed [24]. Acidic drying-wetting conditions also alter pore characteristics, mineral composition, and strain behavior in coal-rock composites [25]. Moreover, in composites made from recycled polyolefins and linen waste, irreversible changes in mechanical properties occur after several sorption-desorption cycles, mainly due to partial failure of the fiber-matrix interface [26]. The mechanical and microstructural evolution of weathered granite soil is also influenced by weathering degree, which affects interparticle friction and cohesion [27]. Advanced techniques such as nuclear magnetic resonance, triaxial testing, and SEM have been employed to study the relationship between pore characteristics and shear strength in granite residual soil under drying-wetting cycles, providing further insight into the underlying microscopic mechanisms [28].

In summary, existing studies confirm that drying-wetting cycles cause meso-structural changes in soils and rocks, which in turn alter their mechanical behavior. However, existent research primarily focuses on natural geomaterials like loess, expansive soil, and clay. As waste slag formed after mineral resource processing, tailings differ significantly from natural soils in terms of properties, particle size distribution, and particle shape. Therefore, this paper takes lead-zinc tailings from a tailings dam in Hunan Province as the research object. Self-designed dry-wet cycle apparatus simulates the absorption-desorption process of tail-

ings in the natural environment. Combined with triaxial shear tests and stereomicroscope observation, this study analyzes the impact of dry-wet cycles on the mechanical properties of tailings, revealing the evolution law of its meso-fabric, and ultimately clarifying the meso-driven mechanisms behind the degradation of macroscopic mechanical properties in tailings. This provides a scientific basis for the long-term safe operation and stability enhancement of tailings dams.

2. Materials and Methods

2.1. Test Materials

The tailings used in this study were collected from a lead-zinc tailings dam in Hunan Province of China. After drying, standard sieve analysis was conducted, and the measured particle size distribution curve is shown in Figure 1. The gradation parameters are as follows: effective particle size d_{10} = 0.078 mm, median particle size d_{30} = 0.158 mm, constrained particle size d_{60} = 0.202 mm, uniformity coefficient Cu = 2.59, and curvature coefficient Cc = 1.584.

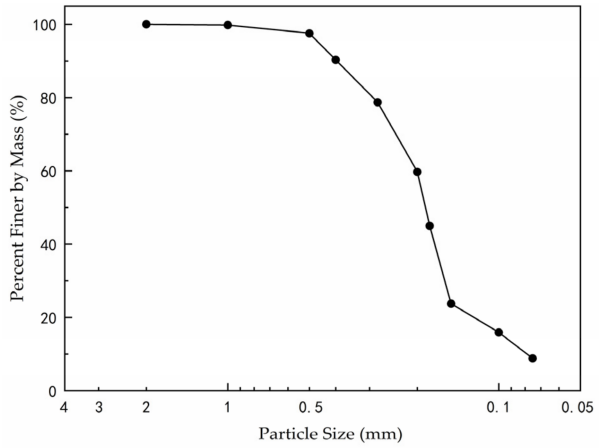

Figure 1. Particle size distribution curve of the tailings.

The basic physical properties of the tailings were determined through standard geotechnical laboratory tests, as shown in Table 1.

Table 1. Gradation parameters.

Natural Water Content ω (%)	Natural Dry Density ρ (g·cm^{-3})	Optimum Moisture Content ω_{op} (%)	Maximum Dry Density ρ_d (g·cm^{-3})	Specific Gravity G_s	Void Ratio e
14.0	1.541	18.2	1.79	2.70	0.752

To determine the mineral composition of the tailings used in this study, X-ray diffraction analysis (XRD) was conducted on the samples, revealing a complex diffraction pattern characteristic of a multi-mineral assemblage. The primary mineral phases identified were quartz, calcite, and muscovite. Sulfide minerals were predominantly represented by pyrite, sphalerite, and galena, with a notable presence of fluorite and other minor accessory minerals.

2.2. Test Equipment

To simulate the actual dry-wet cycle process of tailings in the tailings pond while minimizing disturbance during the experiment, a self-designed dry-wet cycle device made of acrylic material was used, as shown in Figure 2. The device has a diameter of 39.1 mm, with a height of 100 mm, greater than the standard triaxial specimen height of 80 mm, to

facilitate tailings specimen preparation and the wetting process. The shear test used a fully automatic strain-controlled triaxial apparatus. The meso-test employed a stereomicroscope equipped with a color CCD sensor for image data acquisition.



Figure 2. Dry–wet cycling apparatus (self-made).

2.3. Test Scheme

2.3.1. Specimen Preparation

The tailings samples collected from the site were first air-dried until their weight stabilized. The moisture content was then adjusted to match the natural water content level. After that, the samples were sealed and stored for 24 h to ensure uniform distribution of moisture. For the triaxial test specimens, the study employed a compaction method with four layers. Each layer was compacted 20 times. Through a series of preliminary tests, the study confirmed that this compaction effort consistently produced a dry density (1.541 g·cm^{-3}) equivalent to that of the in situ tailings. To protect the specimen surface from potential erosion during the subsequent water absorption phase, a circular piece of filter paper was placed on top of the specimen.

2.3.2. Dry-Wet Cycle Test

Based on the local climatic conditions of the tailings dam and the maximum saturation degree of the tailings, the wet-dry cycle was set with a moisture content amplitude ranging from 1% (the desorption endpoint) to 23% (the absorption endpoint). During the wetting phase, water was slowly added dropwise to the surface of the specimen using a syringe. A filter paper was used to help distribute the water evenly across the surface. After watering, the specimen was sealed and allowed to stand for 24 h to ensure full and uniform water infiltration. For the drying phase, the specimen was placed in a constant-temperature drying oven set at 38.7 °C. To ensure uniform drying and minimize the effects of any temperature gradients inside the oven, the position of the specimen was rotated every two hours. The drying process continued until the water content dropped below 1%. Completing one desorption–absorption process (water content from 14.0% → 1% → 23% → 14.0%) constituted one dry-wet cycle. According to existent research, the mechanical properties and mesostructure of geomaterials tend to stabilize gradually after six wet-dry cycles, while for some materials, the mechanical parameters show a significant decrease after only five cycles. Therefore, in this experiment, a total of six cycles were provisionally selected [29–31]. Specimens with 0 (DW0), 1 (DW1), 2 (DW2), 3 (DW3), 4 (DW4), 5 (DW5), and 6 (DW6) cycles were prepared, with 3 parallel specimens per group to ensure test reliability. In this study, the initial water content was set at 14.0%, which is based on the average natural water content measured from field samples, aiming to simulate the initial moisture condition of tailings in their natural accumulation state. The drying-wetting cycle amplitude was set

between 1% and 23%, primarily for the following considerations: taking into account local climatic characteristics and tailings saturation tests, 23% is close to the saturated water content of the tailings, simulating an extreme wet state; while 1% corresponds to an extreme dry state. This range covers the extreme drying and wetting conditions that tailings may experience in actual environments, facilitating the investigation of the evolution laws of their mechanical properties under the most adverse climatic scenarios.

2.3.3. Macroscopic Mechanical Test

After each set of specimens completed the predetermined number of wet-dry cycles and was demolded, consolidated undrained (CU) triaxial tests were conducted without delay. The tests employed confining pressures of 100, 200, and 300 kPa, which were selected to represent the in situ stress states at typical depths within a tailings dam. During shearing, the study continuously recorded the axial strain, deviator stress, and pore water pressure. The resulting data were used to construct the stress-strain and pore pressure-strain relationships. Based on these curves, the static strength characteristics were evaluated, and the key shear strength parameters were subsequently determined. The shear failure process of the tailings specimen is illustrated in Figure 3.

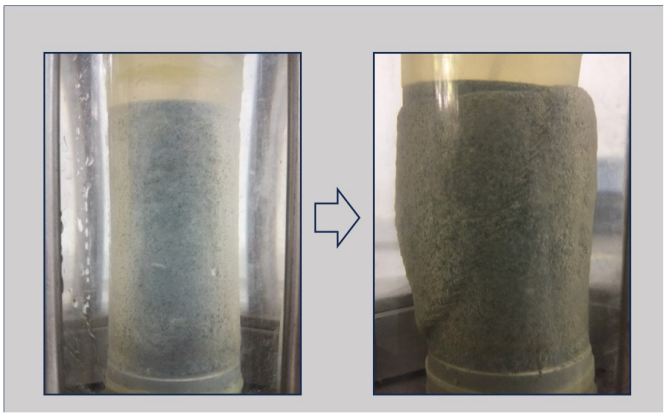

Figure 3. Schematic diagram of the specimen before and after failure.

2.3.4. Meso-Test

To prepare specimens for microstructural observation, fresh sections of the tailings were obtained through a controlled breaking method, which minimizes particle rotation and fabric disturbance that could be induced by mechanical cutting. Representative sections were selected from both the first compaction layer (designated as the upper layer) and the third compaction layer (designated as the lower layer) for imaging under a stereomicroscope. For each sectional surface, three distinct locations were imaged to account for local heterogeneity. Additionally, images were collected from three parallel specimens to effectively reduce the influence of local heterogeneity and ensure representative analysis. Image preprocessing was performed using Image-Pro Plus 6.0 software. The initial step involved histogram equalization (implemented through the "histeq" function) to standardize grayscale distribution and enhance the discernibility of particle-pore boundaries. Following contrast enhancement, a 3×3 kernel median filter was applied using the OpenCV 3.2 library in Python 3.0. This filtering process effectively reduced image noise while preserving critical structural boundaries and avoiding excessive blurring of microstructural features. Subsequently, binarization processing was performed using an adaptive threshold (Domain averaging method) to segment the image into white particle areas and black pore areas. Finally, meso-parameters were extracted and statistically analyzed, including particle size

distribution (equivalent diameter method), porosity (pore area/total image area × 100%), and pore size distribution (equivalent pore diameter method).

3. Influence of Dry-Wet Cycles on Macroscopic Mechanical Properties of Tailings

3.1. Stress-Strain Relationship

The stress-strain curves obtained from the tests of the tailings under different numbers of dry-wet cycles all exhibited strain-softening characteristics, as shown in Figure 4. That is, the deviator stress increases with axial strain to a peak value and then gradually decreases, which is consistent with the poor gradation of the tailings and the susceptibility of particle interlocking to damage during shearing. As the confining pressure increased, the curves transitioned from weak softening to strong softening types, and the peak stress significantly increased, indicating that confining pressure has a significant strengthening effect on tailings strength.

Based on the evolutionary characteristics of the curves, the stress-strain relationship can be divided into four stages: slow growth, linear growth, decelerating growth, and post-peak stages.

During the initial compaction stage (approximately 0–1% axial strain), the deviator stress increases gradually. This stage mainly involves fine particles filling the interparticle voids under load, while the specimen exhibits relatively weak resistance to deformation. This characteristic becomes more pronounced under higher confining pressure due to enhanced particle compression. The subsequent linear elastic stage (1–4% axial strain) shows an essentially linear relationship between deviator stress and axial strain. By this phase, the pore structure has been largely compacted, and the resistance to deformation is primarily governed by interparticle friction and interlocking. Interestingly, the slope of this linear segment demonstrates a distinct "increase-decrease-increase" pattern with successive dry-wet cycles: reaching its maximum at DW1, decreasing noticeably during DW2-DW3, and gradually recovering from DW4 onward. This pattern effectively reflects how dry-wet cycles influence the elastic deformation characteristics of the tailings.

The phenomenon reflects the phased reconstruction of the meso-fabric within the tailings under drying-wetting cycles. The increase in slope after the first cycle (DW1) primarily originates from the temporary enhancement of capillary forces during water absorption and the initial adjustment and compaction of particles under the lubricating effect of moisture, leading to a transient increase in stiffness during the small-strain stage. The subsequent decrease in slope after 2–3 cycles (DW2–DW3) indicates that the accumulation of damage begins to dominate: repeated drying and wetting disrupts interparticle cementation, promotes the disintegration of particle aggregates, and facilitates the development of micro-cracks, resulting in overall structural softening and reduced stiffness. The recovery of slope after the fourth cycle (starting from DW4) does not signify a recovery of strength but rather reflects the collapse of the original unstable skeleton, followed by particle rearrangement and the formation of a geometrically denser yet more weakly cemented "vulnerable new structure." This structure exhibits higher sliding resistance at small strains, but its subsequent load-bearing capacity and deformation stability deteriorate significantly, consistent with the intensified strain softening observed in later stages as discussed subsequently. This evolution process profoundly reveals the macro-meso mechanism of tailings structure transitioning from "adjustment" to "damage" and then to "reorganization and degradation" under drying-wetting cycles.

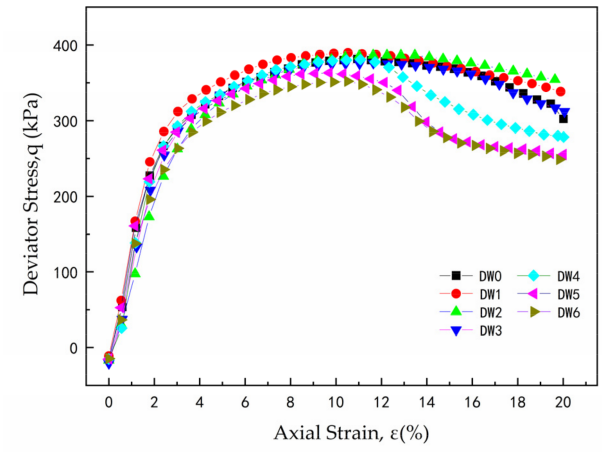

(**a**) σ_3 = 100 kPa

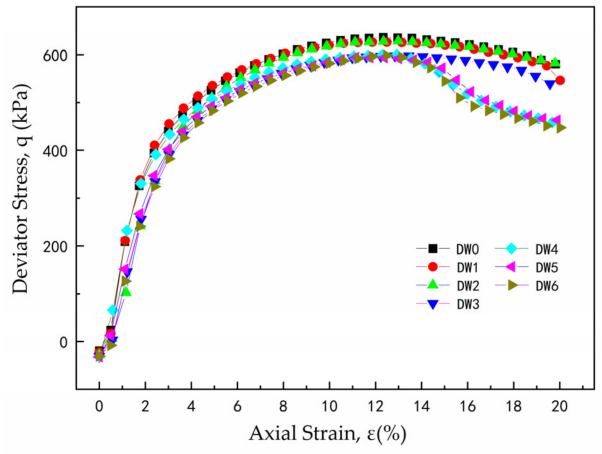

(**b**) σ_3 = 200 kPa

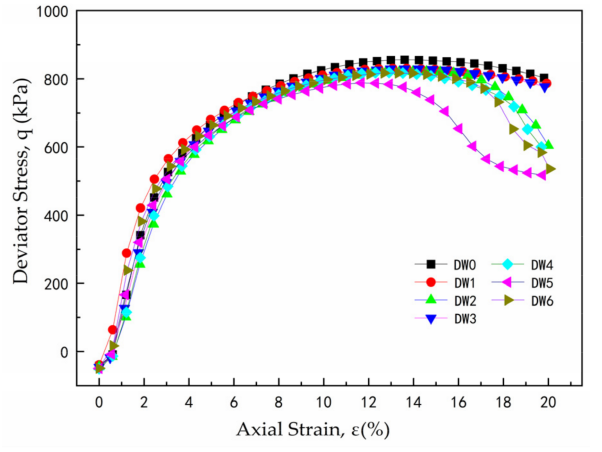

(**c**) σ_3 = 300 kPa

Figure 4. Stress–strain relationship curves.

The plastic yielding stage is where the deviator stress growth rate gradually decreases until the peak. The axial strain corresponding to the peak stress fluctuated roughly in a "W" shape under the influence of dry-wet cycles, as shown in Figure 5, being largest at DW2 and smallest at DW5, indicating significant differences in the plastic deformation capacity of the tailings at different cycle stages.

In the post-peak softening stage, the integrity of the specimen is compromised, and the deviator stress gradually decreases from the peak. The curve decline was gentle during DW0–DW3, indicating weak strain softening. During DW4–DW6, the curve dropped sharply, indicating significant strain softening, likely because internal pores became con-

nected in the later cycles, significantly weakening the interparticle connection force, leading to a rapid decrease in bearing capacity after shear failure.

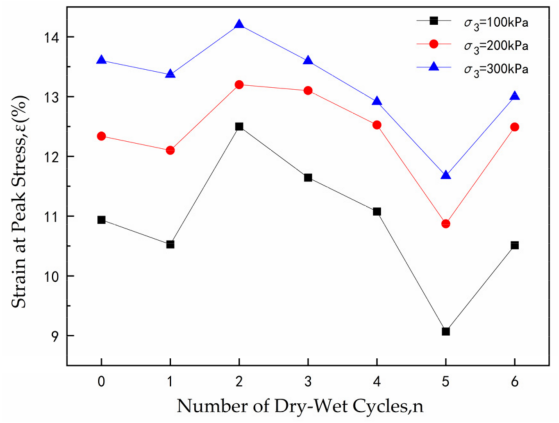

Figure 5. Development curve of axial strain corresponding to peak stress under different confining pressures.

3.2. Pore Water Pressure Changes

In triaxial tests, the variation in pore water pressure can also, to some extent, reflect the strength characteristics of the soil. The relationship between pore water pressure and axial strain was obtained from consolidated undrained shear tests on the seven groups of specimens (DW0–DW6), as shown in Figure 6.

From the perspective of the influence of dry-wet cycles, the location of the peak pore water pressure for specimens with different cycle numbers was relatively fixed. The peak pore water pressure occurred at axial strains of 2.5–3% (σ_3 = 100 kPa), 3–4% (σ_3 = 200 kPa), and 4.5–5.5% (σ_3 = 300 kPa), respectively. Under the same confining pressure, specimens subjected to different numbers of dry-wet cycles showed small variations, indicating that the stage of strongest shear contraction tendency is less affected by the number of cycles and more related to the confining pressure. However, when the specimens underwent DW2, DW3, and DW6 stages, the peak pore pressure was higher than in other stages, indicating that after 2, 3, and 6 dry-wet cycles, the degree of shear contraction caused by the shear test was more obvious. This phenomenon also indicates more intense changes in the internal pore structure of the tailings during these three cycle stages, resulting in greater pore volume compression during shear contraction, further confirming the stage differences in macroscopic mechanical properties.

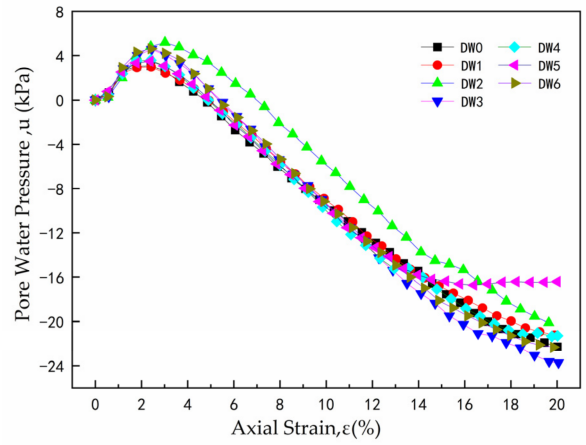

(**a**) σ3 = 100 kPa

Figure 6. *Cont.*

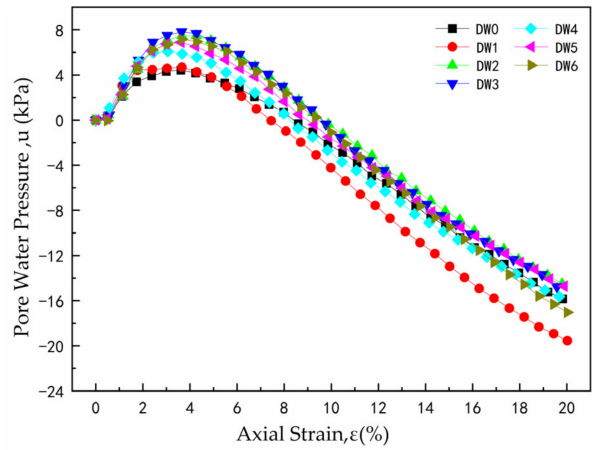

(**b**) σ_3 = 200 kPa

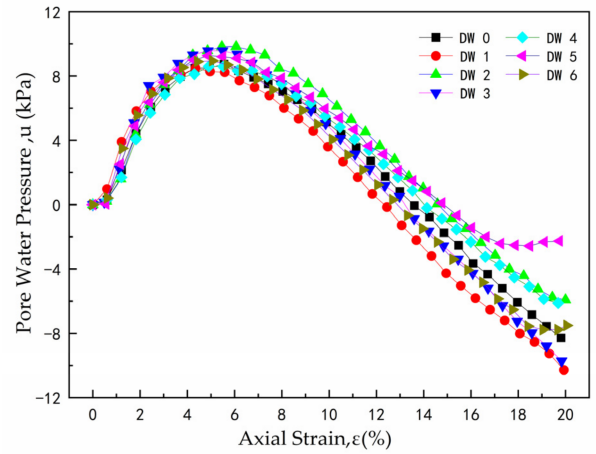

(**c**) σ3 = 300 kPa

Figure 6. Pore pressure-strain relationship curves under the influence of dry-wet cycles.

3.3. Static Strength Changes

The variation in the static strength of the tailings (peak deviator stress from the stress-strain curve) with the number of dry-wet cycles is shown in Figure 7. Overall, under the same confining pressure, the static strength varied slightly with increasing cycle number but generally showed a trend of "initial gradual degradation → temporary recovery → further deterioration".

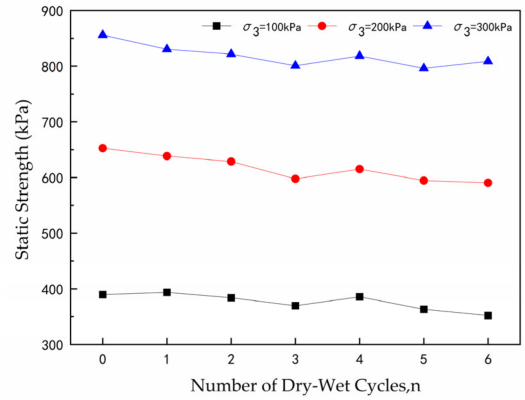

Figure 7. Static strength versus number of dry-wet cycles curves under different confining pressures.

In the early stage of cycling (DW0–DW3), the static strength of the tailings continuously decreased, with the largest decrease occurring during DW2–DW3. Under 100 kPa confining pressure, the static strength of the DW3 specimen decreased by 5.13% compared to DW0;

under 300 kPa, it decreased by 6.45%. The main reason for the strength decrease in this stage is that repeated water infiltration causes fine particles in the tailings to gradually develop cohesion while filling pores, forming relatively loose particle aggregates that are easily broken during shearing, reducing the overall bearing capacity of the tailings. Simultaneously, micro-cracks generated during the desorption process gradually expand, further weakening the interlocking effect between particles.

During the intermediate stage of dry-wet cycling (DW3 to DW4), a slight recovery in static strength was observed. At a confining pressure of 100 kPa, the static strength of DW4 specimens increased by 4.33% compared to DW3, while under 300 kPa, the increase was 2.2%. This recovery pattern can be attributed to microstructural collapse and subsequent reorganization within the tailings. After three dry-wet cycles, the stability of the initial particle skeleton—particularly the force-chain network formed by larger particles—had been significantly compromised. During the fourth wetting phase, water infiltration induced localized collapse of the weakened structure, prompting particle rearrangement and leading to localized densification. This process resulted in a slight reduction in porosity, which in turn contributed to the temporary recovery of static strength observed at this stage.

In the later stage of cycling (DW4–DW6), the static strength showed a renewed declining trend, reaching the lowest after six cycles. Under 100 kPa confining pressure, the static strength of the DW6 specimen decreased by 8.71% compared to DW4 and by 9.65% compared to DW0. Under 300 kPa confining pressure, it decreased by 1.17% compared to DW4 and by 5.51% compared to DW0. The core reason for the strength decrease in this stage is that repeated dry-wet cycles form connected pores inside the tailings. Fine particles and cementitious materials migrate to the specimen surface with water, forming a "bonding layer" as Figure 8, leading to a significant weakening of the interparticle cementation force and friction inside, resulting in continuous degradation of bearing capacity. A brief analysis of this "bonding layer" indicates that its formation primarily occurs during the absorption phase, where water acts as a transport medium, gradually carrying cementitious materials upward. Subsequently, during the desorption phase, capillary forces draw fine particles toward the surface, leading to the aggregation and formation of the bonding layer. This layer is mainly composed of accumulated fine particles and precipitated soluble cementitious substances. It is inferred to possess low strength, brittleness, and moisture-sensitive mechanical properties.



Figure 8. Bonding layer on the surface of the specimen after multiple dry-wet cycles.

3.4. Shear Strength Parameter Changes

The shear strength of tailings depends on various factors, but in practical applications, the Mohr-Coulomb failure criterion is still widely used, describing the shear strength using

effective cohesion c′ and effective internal friction angle φ′. These two parameters for tailings subjected to different numbers of dry-wet cycles can be calculated by plotting Mohr strength envelopes, with the results shown in Figure 9.

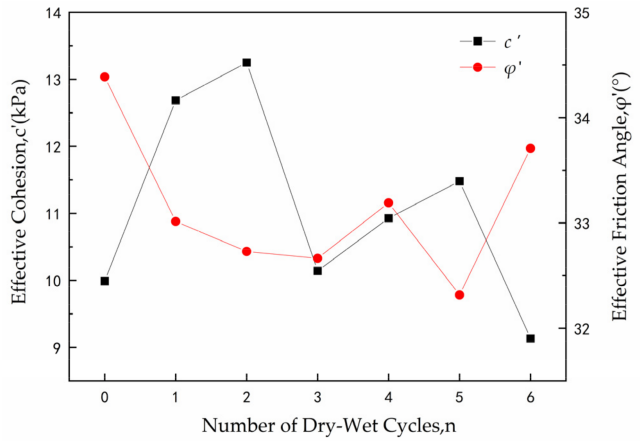

Figure 9. Variation curves of c′ and φ′ with dry-wet cycles.

As can be seen from the figure, the effective cohesion c′ fluctuated in an "M" shape with increasing number of dry-wet cycles, with a maximum variation amplitude of 31.1%: it was highest at the DW2 stage, 32.6% higher than DW0; lowest at the DW6 stage, 8.6% lower than DW0; showed a slight recovery during DW4–DW5, but then a clear downward trend after the DW6 stage. Analyzing the reasons, the fluctuation of c′ is mainly related to changes in interparticle cementation force and water film attraction. In the early cycles (DW0–DW2), water infiltration increases the thickness of the water film on particle surfaces, enhancing intermolecular attraction, while the particle aggregates formed by the cohesion of fine particles provide additional cementation, thus c′ increases. In the middle cycles (DW2–DW3), the breakdown of particle aggregates and the migration of cementitious material to the specimen surface lead to weakened cementation, causing a significant decrease in c′. In the later cycles (DW3–DW6), particle reorganization and densification cause a temporary recovery of c′, but the formation of connected pores and the loss of cementitious material ultimately lead to a renewed decrease in c′, with the potential for further reduction if dry-wet cycles continue.

The effective internal friction angle φ′ roughly fluctuated in a "W" shape with the number of dry-wet cycles, but the overall variation was small, only 6.02%. It was highest at the DW0 stage and lowest at the DW5 stage, showing a continuous decrease from DW0 to DW5, with a slight increase at the DW4 stage, and then an increase back to 33.71° at the DW6 stage. The small variation in φ′ is primarily because φ′ is determined by particle surface friction and interparticle interlocking. The particle morphology (mainly angular) and gradation of the tailings did not change significantly during the dry-wet cycles, only the particle arrangement was slightly adjusted, so φ′ remained generally stable. However, in the early and middle stages of cycling, under the action of water, fine particles and cementitious materials in the tailings gradually cohere, making the internal structure of the tailings looser and unstable, leading to easier sliding between particles. Therefore, as the dry-wet cycles progress, the internal friction angle of the tailings decreases slightly. During the DW3–DW4 stage, due to possible internal structural collapse of the tailings, the volume shrinks slightly, subsequently reducing porosity and strengthening particle interlocking, resulting in a small increase in φ′ during this stage. As the dry-wet cycles proceed, the pore structure of the tailings gradually stabilizes, and fine particles and cementitious materials float up to the specimen surface. This gradual development may cause a slight decrease in

the internal friction angle before the pore structure stabilizes, but after stabilization, the interlocking effect between particles strengthens, leading to a small recovery.

4. Influence of Dry-Wet Cycles on Meso-Fabric of Tailings

4.1. Particle Size Distribution Characteristics

Image-Pro Plus software was used to extract particle size distribution data from sections of the 1st and 3rd layers of tailings specimens after different numbers of cycles. The results are shown in Figure 10. Since the first layer is directly exposed to drying-wetting cycles, serving as the primary zone for water infiltration, evaporation, and fine-particle migration, while the third layer is situated between the second and fourth layers, it best represents the structural response of the internal bulk of the specimen. During the experiments, data from the second layer of some specimens were also collected. Preliminary tests indicated that the evolution trends of mesoscopic parameters in the second layer fall between those of the first and third layers, and its behavior can be reasonably inferred from the trends observed in the adjacent layers. To focus resources on the most representative regions for in-depth analysis, this study primarily concentrates on the first and third layers.

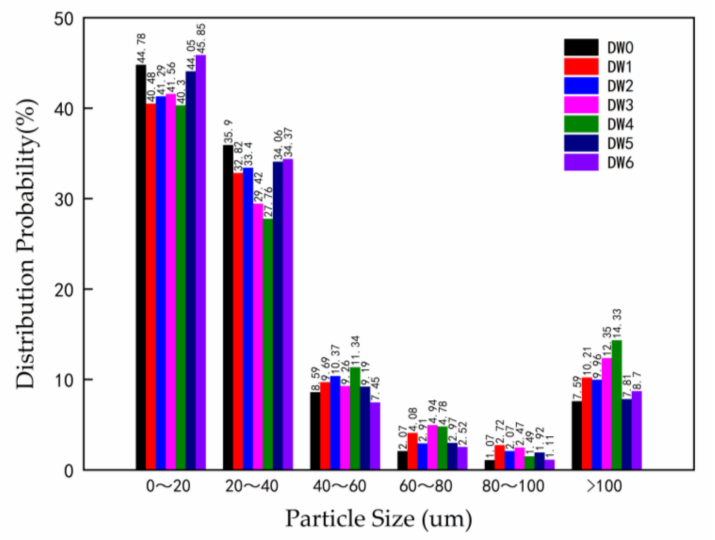

(**a**) First layer

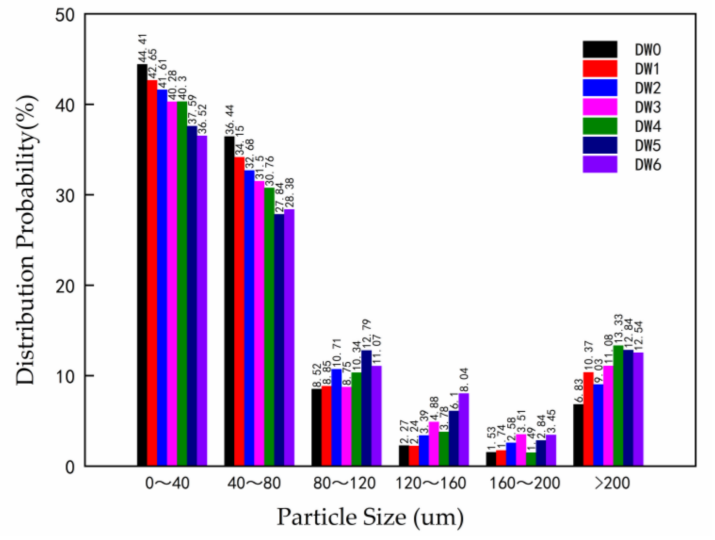

(**b**) Third layer

Figure 10. Cross-sectional particle size distribution in the (**a**) first layer (**Upper**) and (**b**) third layer (**Lower**) after different dry-wet cycles.

As can be seen from the figure, the particle sizes in the tailings sections are mostly concentrated in the ranges of 0–120 μm and above 200 μm, while the content of intermediate-sized particles (120–200 μm) is relatively low. This result differs somewhat from the sieve analysis results, possibly because during image processing, fine particles extensively adsorb around large particles, increasing the probability distribution of fine particles.

In the first layer (upper layer), the proportion of fine particles (0–40 μm) showed a trend of "decrease—recovery" with increasing cycle number. The proportion was 44.78% at DW0, decreased to 41.56% at DW3, and recovered to 45.85% at DW6. This trend corresponds to the change in macroscopic static strength. During DW0–DW3, fine particles migrated downward with water and filled lower layer pores, so the proportion of fine particles in the upper layer decreased. During DW3–DW6, structural collapse caused fine particles from the lower layer to migrate upward again, generating a bonding layer on the specimen surface, so the proportion of fine particles in the upper layer recovered.

In the third layer (lower layer), the proportion of fine particles continuously decreased with increasing cycle number, while the proportion of large particles increased. This phenomenon indicates that despite staged particle back-migration, long-term dry-wet cycles still cause fine particles to continuously migrate from the lower layer to the upper layer, ultimately leading to further degradation of the particle size distribution in the lower layer, with a more prominent skeleton structure dominated by large particles.

4.2. Porosity Changes

In the triaxial shear test of tailings, porosity has a significant influence on both elastic and plastic deformation as well as mechanical properties. In image analysis, porosity was calculated using "Pore Area/Total Image Area × 100%". The variation law of meso-porosity with the number of dry-wet cycles was compiled, as shown in Figure 11.

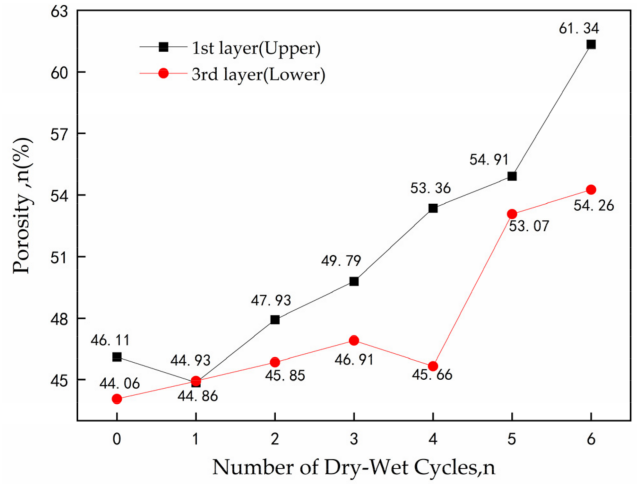

Figure 11. Porosity variation curves with number of dry-wet cycles for the first (**Upper**) and third (**Lower**) layers.

Since the tailings specimens were prepared using layered compaction, without undergoing cycles, the lower layer tailings have lower porosity and higher density compared to the upper layer. As the cycles proceed, the porosity of both the first and third layers of the specimen overall shows an increasing trend. However, the first layer porosity slightly decreased after 1 cycle, and the third layer porosity also decreased somewhat after the fourth cycle. The reason for the decrease in first layer porosity at the DW1 stage may be that the initial absorption expels air from between particles in the upper layer, and fine particles fill tiny pores. However, repeated dry-wet cycles lead to the breakdown of particle aggregates and the formation of connected pores. Simultaneously, the surface bonding

layer hinders water penetration, causing pore water pressure to build up and exacerbating pore expansion. In the lower layer during the early cycles, the repeated action of water enhances the cohesion between fine particles, leading to an increase in porosity. During the middle cycles, particles temporarily rearrange and densify, causing slight volume shrinkage of the specimen, resulting in a temporary decrease in porosity. However, after repeated absorption and desorption processes, by the later cycles, irreversible changes occur in the internal fissures of the specimen, porosity increases significantly and has the potential to further increase with continued dry-wet cycles.

4.3. Pore Size Distribution Characteristics

Porosity reflects the overall void ratio of the specimen but cannot describe the specific pore size distribution. By further analyzing the image files, the pore size and its distribution probability under the action of dry-wet cycles were plotted, as shown in Figure 12.

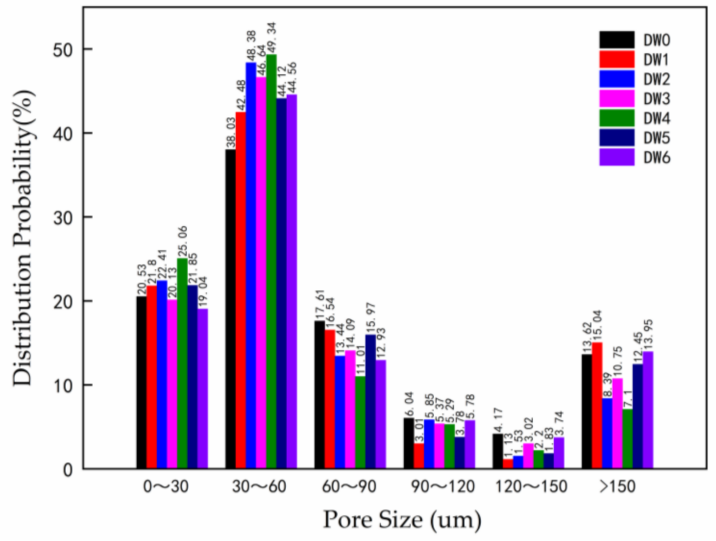

(**a**) First layer

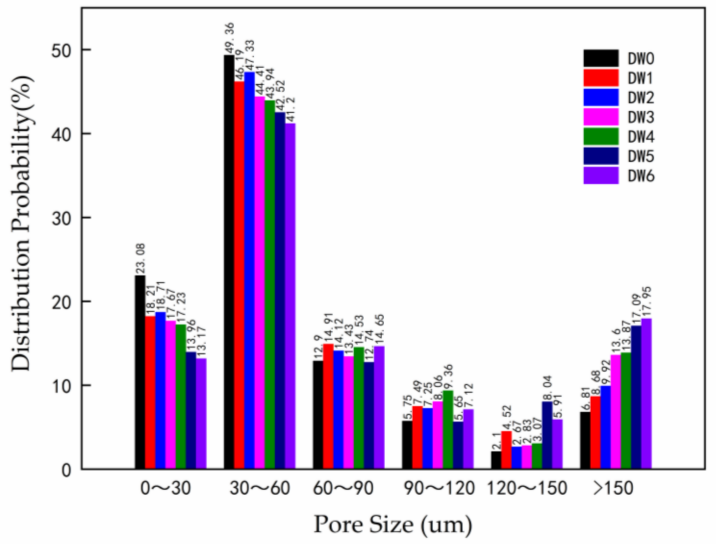

(**b**) Third layer

Figure 12. Pore size distribution in the (**a**) first layer (**Upper**) and (**b**) third layer (**Lower**) after different dry-wet cycles.

Pores were classified into three categories based on size: small pores (<60 μm), medium pores (60–150 μm), and large pores (>150 μm). This classification was adopted primarily because the pores in this tailings material are predominantly distributed within two ranges:

below 60 μm and above 150 μm. Thus, selecting 60 μm and 150 μm as the classification thresholds naturally aligns with the inherent pore system characteristics of the material, facilitating effective tracking of the evolution of its dominant pore types.

In the upper layer of the specimen, the proportion of small pores first increased and then decreased with increasing cycle number, while the proportion of large pores showed the opposite trend, first decreasing and then increasing. The proportion of medium pores changed relatively little. This pattern indicates that in the early cycles, under the action of water, fine particles cohere and float upward, and this filling effect increases the number of small pores. In the later cycles, the gradual formation of connected pores leads to large pores becoming dominant, thus increasing the distribution probability of large pores. In the lower layer of the specimen, the proportion of small pores continuously decreased with increasing cycle number, while the proportion of large pores continuously increased. The distribution probability of medium pores was similar to that in the upper layer, with a small range of variation. This phenomenon further confirms the continuous loss of fine particles in the lower layer and the evolution of pores towards larger sizes.

4.4. Macro-Meso Correlation Mechanism

Combining the analysis of macroscopic mechanical properties and meso-fabric, the macro-meso correlation mechanism of tailings under dry-wet cycles can be established.

The "initial gradual degradation → temporary recovery → further deterioration" of tailings static strength under dry-wet cycles is closely coupled with meso-particle migration and skeleton reorganization. In the early stage of cycling (DW0–DW3), fine particles (0–40 μm) in the upper layer migrate downward with water, forming loose particle aggregates that are easily broken during shearing, leading to a certain degree of decrease in static strength, while porosity increases synchronously. In the middle stage (DW3–DW4), the collapse of the initial skeleton promotes particle rearrangement and densification, lower layer porosity decreases, and static strength recovers slightly. In the later stage (DW4–DW6), connected pores form, fine particles aggregate on the surface to form a low-strength bonding layer, and static strength decreases by 5.51–9.65% compared to the initial state.

The evolution of pore structure directly regulates shear strength parameters and deformation characteristics. The effective cohesion c' fluctuates in an "M" shape. In the early stage, due to thickened particle water films and small pore filling, c' increases slightly. In the middle stage, pore expansion causes c' to decrease with some fluctuation. In the later stage, connected pores cause c' to decrease again. The effective internal friction angle φ' fluctuates in a "W" shape with a small amplitude of only 6.02%, because the angular particle morphology and gradation are stable, and only minor pore adjustments affect the interlocking effect. The softening characteristics of the stress-strain curve are also related to pore size distribution. In the early stage, small pores dominate, showing weak softening. In the later stage, the proportion of large pores increases, showing strong softening. The magnitude of the peak pore water pressure is also influenced by the pore size distribution.

In summary, the synergistic evolution of tailings' macro-meso characteristics can be divided into three stages: the Initial Degradation Stage (DW0–DW3), where particle migration leads to skeleton loosening and macroscopic strength decrease; the Temporary Recovery Stage (DW3–DW4), where particle reorganization and densification cause strength recovery; and the Deep Degradation Stage (DW4–DW6), where pore connection coupled with the formation of a surface bonding layer leads to a significant decrease in strength. This correlation mechanism indicates that the macroscopic mechanical response is the external manifestation of meso-fabric adjustment, providing theoretical support for the stability assessment and reinforcement of tailings dams.

5. Conclusions

Through systematic drying-wetting cycle experiments, triaxial shear tests, and meso-scale image analysis, this study reveals the synergistic evolution patterns and intrinsic mechanisms of the macroscopic mechanical properties and meso-fabric of metal tailings under drying-wetting cycles. The main conclusions are as follows:

(1) At the macroscopic level, drying-wetting cycles did not alter the strain-softening type of the stress-strain curves of the tailings, but significantly intensified the degree of strain softening in the later cycles (four–six cycles). The static strength generally decreased with increasing number of cycles. After six cycles, the strength under 100 kPa confining pressure decreased by 21.2% compared to the initial state, with the largest reduction occurring in the mid-stage (2–3 cycles). A slight recovery was observed at the fourth cycle. The variation amplitude of effective cohesion (31.09%) was much larger than that of the effective internal friction angle (6.02%), indicating that drying-wetting cycles have a more pronounced influence on cohesion.

(2) Regarding meso-fabric evolution, drying-wetting cycles caused upward migration of fine particles (0–60 μm) in the tailings, leading to a notable decrease in the proportion of fine particles in the third layer after six cycles. Porosity increased overall, with the third layer rising from 44.06% to 54.26%. Pores evolved toward a dominance of large pores (>150 μm), and the proportion of large pores in the 3rd layer increased significantly.

(3) A three-stage conceptual model for damage evolution under drying-wetting cycles was established, applicable to poorly graded metal tailings, clarifying the causal chain between macroscopic mechanical responses and meso-structural reconstruction in different stages:

Structural adjustment stage (initial, one–three cycles): Water infiltration induces fine-particle migration and capillary cementation, manifested macroscopically as a slight decrease in strength and stiffness that first increases then decreases.

Damage accumulation stage (mid-term, three–four cycles): Repeated swelling and shrinkage disrupt cementation, promote micro-crack development, and transform small pores into medium-large pores, resulting in a significant reduction in macroscopic strength.

Structural reconstruction and degradation stage (later, four–six cycles): The particle skeleton collapses and rearranges, forming a "low-strength new steady state" characterized by connected large pores and a surface bonding layer, which macroscopically exhibits continued strength decline and intensified strain softening.

(4) From the meso-scale perspective, this study elucidates that the serial physical process of "fine-particle migration-pore interconnection-cementation loss" serves as the fundamental driver for the degradation of macroscopic mechanical properties, overcoming previous limitations that primarily focused on empirical macroscopic descriptions of drying-wetting effects. The proposed three-stage evolution model not only reveals the nonlinear and phased characteristics of tailings performance degradation but also mechanistically explains complex phenomena such as the "temporary strength recovery". It provides a meso-mechanical basis for the long-term stability assessment and risk control of tailings dams under changing climatic conditions.

Author Contributions: Conceptualization, P.A. and Z.Z.; investigation, data curation, P.A., Y.T., M.W. and Z.L.; writing—original draft preparation, P.A.; supervision, writing—review and editing, Z.Z. All authors have read and agreed to the published version of the manuscript.

Funding: The work is funded by the National Natural Science Foundation of China (52274167), Key Research Project Supported by Hunan Provincial Department of Education (23A0329), Young Scientists Fund Project of Hunan Provincial Natural Science Foundation (2023JJ40549).

Institutional Review Board Statement: Not applicable.

Informed Consent Statement: Not applicable.

Data Availability Statement: The original contributions presented in this study are included in the article. Further inquiries can be directed to the corresponding author.

Conflicts of Interest: The authors declare no conflicts of interest.

References

1. Torres-Cruz, L.A.; O'Donovan, C. Public remotely sensed data raise concerns about history of failed Jagersfontein dam. *Sci. Rep.* **2023**, *13*, 4953. [CrossRef] [PubMed]
2. Owen, J.R.; Kemp, D.; Lèbre, É.; Svobodova, K.; Pérez Murillo, G. Catastrophic tailings dam failures and disaster risk disclosure. *Int. J. Disaster Risk Reduct.* **2020**, *42*, 101361. [CrossRef]
3. de Lima, R.E.; de Lima Picanço, J.; da Silva, A.F.; Acordes, F.A. An anthropogenic flow type gravitational mass movement: The Córrego do Feijão tailings dam disaster, Brumadinho, Brazil. *Landslides* **2020**, *17*, 2895–2906. [CrossRef]
4. Tole, I.; Delogu, F.; Habermehl-Cwirzen, K.; Cwirzen, A. Revalorization of Swedish Iron Ore Mine Tailings as Supplementary Cementitious Material through Mechanochemical Activation. *J. Mater. Civ. Eng.* **2025**, *37*, 19878. [CrossRef]
5. Tayebi-Khorami, M.; Edraki, M.; Corder, G.; Golev, A. Re-Thinking Mining Waste through an Integrative Approach Led by Circular Economy Aspirations. *Minerals* **2019**, *9*, 286. [CrossRef]
6. Petronijević, N.; Alivojvodić, V.; Sokić, M.; Marković, B.; Stanković, S.; Radovanović, D. Sustainable mining towards accomplishing circular economy principles. *J. Appl. Eng. Sci.* **2020**, *18*, 493–499. [CrossRef]
7. Wu, L.-L.; Guo, Y.-H.; Tong, K.-W.; Hu, L.; Yu, Q.; Zhang, Z.-J. Mechanical Properties of Tailings Sample with Different Moisture Contents under Dry and Wet Cycles. *Adv. Civ. Eng.* **2019**, *2019*, 9079754. [CrossRef]
8. Rodriguez-Pacheco, R.; Butlanska, J.; González, A.O.O.; Muñoz-Moreno, A. Discharge, Drying and Wetting Cycles of Tailings Dam: Its Effect On Physical, Mechanical and Hydraulic Properties. *Rev. Gestão Soc. Ambient.* **2025**, *19*, e09952. [CrossRef]
9. Guo, P.; Gu, J.; Su, Y.; Wang, J.; Ding, Z. Effect of cyclic wetting-drying on tensile mechanical behavior and microstructure of clay-bearing sandstone. *Int. J. Coal Sci. Technol.* **2021**, *8*, 956–968. [CrossRef]
10. Zhou, Z.; Cai, X.; Chen, L.; Cao, W.; Zhao, Y.; Xiong, C. Influence of cyclic wetting and drying on physical and dynamic compressive properties of sandstone. *Eng. Geol.* **2017**, *220*, 1–12. [CrossRef]
11. Liu, X.; Liu, Q.; Huang, S.; Liu, B.; Liu, J. Effects of cyclic wetting-drying on the mechanical behavior and improved damage model for sandstone. *Mar. Georesources Geotechnol.* **2020**, *39*, 1244–1254. [CrossRef]
12. Wang, Z.; Shi, J.; Ding, K.; Chen, S.; Jiang, X.; Shen, C. Analysis of mechanical properties and deterioration mechanisms of mudstone under wetting-drying cycles. *Mech. Adv. Mater. Struct.* **2024**, *32*, 3337–3344. [CrossRef]
13. Huang, S.; Wang, J.; Qiu, Z.; Kang, K. Effects of Cyclic Wetting-Drying Conditions on Elastic Modulus and Compressive Strength of Sandstone and Mudstone. *Processes* **2018**, *6*, 234. [CrossRef]
14. Cikmit, A.A.; Tsuchida, T.; Takeyama, K.; Hashimoto, R.; Noguchi, T.; Kaya, K. Effects of primary curing and subsequent disturbances on strength development of steel slag-treated marine clay. *Soils Found.* **2021**, *61*, 1287–1301. [CrossRef]
15. Zhao, Y.; Zeng, Z.; Lü, H. The Influence of Water Formation on Mechanical Properties of Soil. *Civ. Eng. Urban Plan.* **2012**, *2012*, 734–737. [CrossRef]
16. Tang, C.-S.; Cheng, Q.; Gong, X.; Shi, B.; Inyang, H.I. Investigation on microstructure evolution of clayey soils: A review focusing on wetting/drying process. *J. Rock Mech. Geotech. Eng.* **2023**, *15*, 269–284. [CrossRef]
17. Roshani, A.; Fall, M.; Kennedy, K. A column study of the hydro-mechanical behavior of mature fine tailings under atmospheric drying. *Int. J. Min. Sci. Technol.* **2017**, *27*, 203–209. [CrossRef]
18. Khan, S.; Ivoke, J.; Nobahar, M. Coupled Effect of Wet-Dry Cycles and Rainfall on Highway Slope Made of Yazoo Clay. *Geosciences* **2019**, *9*, 341. [CrossRef]
19. An, R.; Kong, L.; Zhang, X.; Li, C. Effects of dry-wet cycles on three-dimensional pore structure and permeability characteristics of granite residual soil using X-ray micro computed tomography. *J. Rock Mech. Geotech. Eng.* **2022**, *14*, 851–860. [CrossRef]
20. Liu, W.; Zhang, Z.-H. Experimental characterization and quantitative evaluation of slaking for strongly weathered mudstone under cyclic wetting-drying condition. *Arab. J. Geosci.* **2020**, *13*, 65. [CrossRef]
21. Hao, R.; Zhang, Z.; Guo, Z.; Huang, X.; Lv, Q.; Wang, J.; Liu, T. Investigation of Changes to Triaxial Shear Strength Parameters and Microstructure of Yili Loess with Drying-Wetting Cycles. *Materials* **2021**, *15*, 255. [CrossRef]
22. Zhang, X.; Zhang, X.; Li, J.; Su, L.; Liu, J. Study of the damage mechanism on mechanical properties of super absorbent polymer-improved geopolymers under dry-wet cycling. *J. Mater. Sci.* **2024**, *59*, 4662–4679. [CrossRef]
23. Liu, X.; Huang, F.; Zheng, A.; Hu, X. Micro-dissolution mechanism and macro-mechanical behavior of red-bed soft rock under dry-wet cycle. *Mater. Lett.* **2024**, *362*, 136220. [CrossRef]
24. Yi, Q.; Pu, H.; Preuße, A.; Bian, Z.; Wu, J. Effect of dry-wet cycles on dynamic mechanic and microstructure of cemented broken mudstone. *Constr. Build. Mater.* **2022**, *357*, 129347. [CrossRef]

25. Chen, W.; Liu, B.; Wu, Q.; Zhao, Y.; Wan, W.; Liu, J.; Peng, W. Experimental Investigation of Acidic Dry–wet Cycles on Coal-rock Combination: Mechanical Performance and Microstructural Analysis. *Rock Mech. Rock Eng.* **2025**, *58*, 10315–10357. [CrossRef]
26. Bakradze, G.; Kajaks, J.; Reihmane, S.; Krutohvostov, R.; Bulmanis, V. The influence of water sorption-desorption cycles on the mechanical properties of composites based on recycled polyolefine and linen yarn production waste. *Mech. Compos. Mater.* **2007**, *43*, 573–578. [CrossRef]
27. Wang, Y.; Jia, R.; Li, Y.; Yang, K.; Cui, J.; Shan, Y. Study on the mechanical properties and microscopic evolution mechanisms of weathered granite soil. *Sci. Rep.* **2024**, *14*, 24388. [CrossRef]
28. An, R.; Kong, L.; Li, C. Effects of Drying-Wetting Cycles on the Microstructure and Mechanical Properties of Granite Residual Soils. *Soil Mech. Found. Eng.* **2022**, *58*, 474–481. [CrossRef]
29. Nie, Y.; Ni, W.; Lü, X. Effects of dry-wet cycles on compacted loess: From macroscopic to microscopic investigation. *Eur. J. Environ. Civ. Eng.* **2023**, *28*, 1370–1393. [CrossRef]
30. Ma, T.; Liu, H.; Zou, Q.; Kong, F.; Ran, Q.; Wang, P. Damage evolution characteristics and deterioration mechanism of mechanical properties of sandstone subjected to drying-wetting cycles. *J. Mater. Res. Technol.* **2023**, *23*, 4591–4605. [CrossRef]
31. Tan, H.; Li, J.; Shi, Z.; Wang, M.; Wang, J.; Li, J. Damage evolution and failure characteristics of red sandstone with prefabricated crack under coupled dry-wet cycle-fatigue loading. *Int. J. Fatigue* **2023**, *175*, 107751. [CrossRef]

Disclaimer/Publisher's Note: The statements, opinions and data contained in all publications are solely those of the individual author(s) and contributor(s) and not of MDPI and/or the editor(s). MDPI and/or the editor(s) disclaim responsibility for any injury to people or property resulting from any ideas, methods, instructions or products referred to in the content.